nature materials

SUPPLEMENTARY INFORMATION

DOI: 10.1038/NMAT4696

Reconfiguring active particles by electrostatic imbalance

Jing Yan,[1,+] Ming Han,[2,+] Jie Zhang,[1] Cong Xu,[1] Erik Luijten,[3*] Steve Granick[4*]

[1]Department of Materials Science and Engineering, University of Illinois, Urbana, IL 61801, USA

[2]Applied Physics Graduate Program, Northwestern University, Evanston, IL 60208, USA

[3]Department of Materials Science and Engineering, Engineering Sciences and Applied Mathematics, and Physics and Astronomy, Northwestern University, Evanston, IL 60208, USA

[4]IBS Center for Soft and Living Matter, UNIST, Ulsan 689-798, South Korea

[+]J.Y and M.H. contributed equally to this work.

*E.L.: luijten@northwestern.edu; S.G.: sgranick@ibs.re.kr

DOI: 10.1038/NMAT4696

1. Parameters for the calculation of the dielectric spectra

To calculate the frequency spectra of the dipole coefficients of both hemispheres and their resultant dipolar interactions, we employed the model in Ref. 22. Parameters used in the current study are: Debye length κ^{-1} = 250 nm for deionized water[31] and 30 nm for aqueous 0.1 mM NaCl solution; temperature T = 298 K; relative permittivity of the solvent ε_m = 78.5; viscosity of water $\eta = 0.89\times10^{-3}$ Pa·s. The ζ-potential of the silica surface is measured to be −52 mV. The solution conductivity K_s is calculated via Eq. (25) in Ref. 32, where $D^+ = 9.3\times10^{-9}$ m^2/s corresponds to H^+ (Ref. 33) and $D^- = 1.1\times10^{-9}$ m^2/s corresponds to HCO_3^- (Ref. 34), which are the dominant ionic species present in deionized water due to the absorption of CO_2 from air. For the NaCl solution, we use $D^+ = 1.3\times10^{-9}$ m^2/s and $D^- = 2.0\times10^{-9}$ m^2/s (Ref. 35). Taking into account the protective SiO_2 coating on the metallic surface, the critical frequency ω_c (cf. Eq. (3) in Ref. 36) is increased by a factor $(1+\delta_1)$, where $\delta_1 = \varepsilon d_{SiO_2}\kappa \big/ \varepsilon_{SiO_2}$, with $d_{SiO_2} = 15$ nm being the thickness of the protective coating and $\varepsilon_{SiO_2} = 3.9$ its permittivity. Meanwhile, the magnitude of the dipole moment is reduced by a factor $(1+\delta_2)$, where $\delta_2 = d_{SiO_2}\varepsilon \big/ 2a\varepsilon_{SiO_2}$ (Ref. 37). The parameter Θ, characterizing the contribution of the surface conductivity in the tightly bounded layer relative to that of the diffuse layer, is set to 1.2 (Ref. 38).

2. Dependence of the particle velocity on the electric field frequency and strength

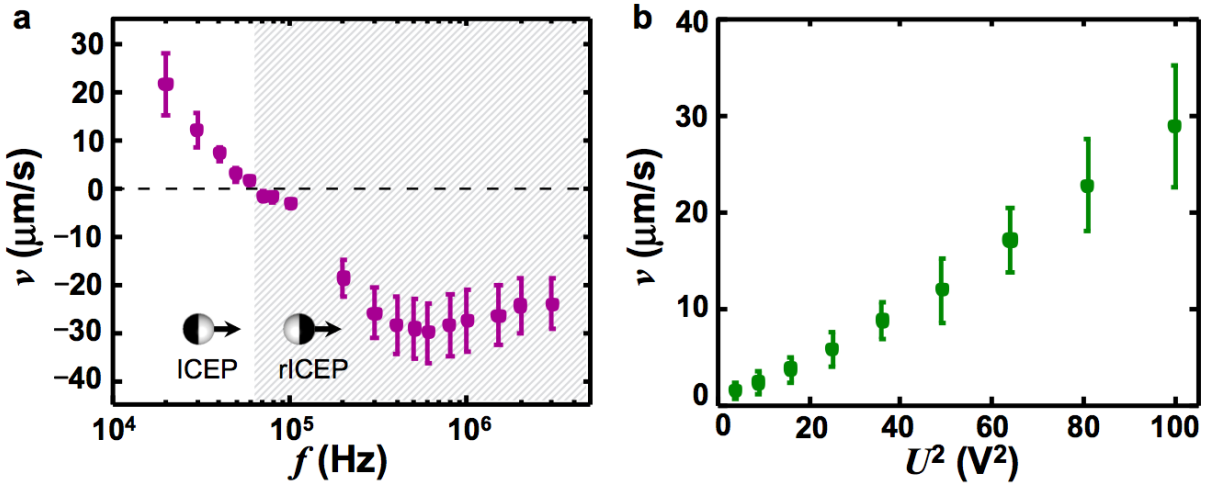

Figure S1. Dependence of the particle swimming velocity on electric field frequency and strength. a, Dependence of particle velocity v on frequency f in an 0.1 mM NaCl solution. The electric field strength is kept constant at 8.33×10^4 V/m. At low frequency, a Janus particle swims with its dielectric side facing forward, a phenomenon known as induced-charge electrophoresis (ICEP, unshaded area). At high frequency, the Janus particle reverses its swimming direction, with the metallic side facing forward, a phenomenon called reversed ICEP (rICEP, shaded area). **b**, Dependence of particle velocity v on the square of the applied voltage, U^2, in an 0.1 mM NaCl solution. The frequency is set to 500 kHz, i.e., in the rICEP region. The velocity v scales quadratically with electric field strength, like the reported dependence for conventional ICEP[15].

Supplementary Fig. S1a shows the frequency dependence of particle velocity in an 0.1 mM NaCl solution. Our measurement is limited to above ~10 kHz by the strong electrohydrodynamic flows in the whole system and to below 4 MHz by the capacitance of the chamber. At low frequency, a metallodielectric Janus particle swims with its dielectric side forward. Such induced-

DOI: 10.1038/NMAT4696

charge electrophoresis (ICEP) relies on slip flows in the electric double layer (EDL), driven by the local electric field tangential to the particle surface. As the frequency f increases, it becomes increasingly difficult for ions to follow the rapidly varying field and to establish a fully charged EDL. As a consequence, the local electric fields gradually become perpendicular to the particle surface to support the charging of the EDL, leading to weaker slip flows. Consistently, the particle velocity v decreases with frequency f. Above a crossover frequency f_0 of ~70 kHz, the Janus particle reverses its swimming direction (moving with the metallic side facing forward). This reversal of particle motion at high frequency has been reported before[39], but the underlying mechanism remains elusive. As the frequency increases further (> MHz), the particle speed eventually drops again. Supplementary Fig. S1b shows the quadratic dependence of particle speed on the applied voltage at frequency f = 500 kHz. Although the particle has reversed direction at this frequency, the quadratic scaling predicted for regular ICEP persists[15].

We observed a similar frequency dependence in deionized water but with a much lower reversal frequency f_0 ~ 10 kHz. This reduction in f_0 is caused by the significant decrease in ion concentration. The charging frequency f_c of the EDL provides a reference frequency for the ICEP, which scales as the square root of the ionic concentration c (Ref. 15). Since c = 1.5 μM for deionized water, f_c is roughly 1/8 of that in an 0.1 mM NaCl solution. Likewise, the reversal frequency reduces from 70 kHz to 10 kHz. Since the ion concentration undergoes large relative changes over time for deionized water, we were not able to perform similar quantification of the velocity directly in deionized water.

3. Characterization of binary collision events in the swarm state

To quantitatively prove that head-to-head repulsions give rise to alignment between the Janus colloids in the swarm state, we experimentally tracked more than 10,000 binary collision events under the same condition as the swarming experiment but at extremely low density ($\phi_0 < 0.01$). A binary collision is defined as a process during which the center-to-center distance between two particles is smaller than a threshold value of $3D$. We have varied this threshold from $2D$ to $4D$; the conclusions below remain qualitatively valid. Consistent with our hypothesis, we observe *transient* alignment between two colliding spheres.

A representative collision event is shown in Supplementary Fig. S2a. The two particles initially rotate toward the same direction as they move closer, and then become maximally aligned at approximately 3/4 through the collision event, and finally their orientations diverge again slightly. To quantify two-particle alignment, we investigate the time evolution of the angle θ between the Janus directors of the two colliding spheres by analyzing this large statistical dataset. As shown in Supplementary Fig. S2b, as time passes the distribution of θ changes from a broad distribution peaked near $\pi/2$ to a sharp peak at 0 (the aligned state) with long tails. By the end of the collision event, the distribution broadens again slightly and the peak at 0 disappears. All these observations are consistent with the picture that the repulsion between the two leading hemispheres gives rise to a torque, which first reorients the two colliding spheres to an aligned configuration but then to a diverging configuration in this dilute system. Note that we only include "effective" collisions in which the two spheres initially point towards a common point. "Ineffective" geometries include passing-by events or head-to-head collisions, which constitute 34% of all collision events.

DOI: 10.1038/NMAT4696

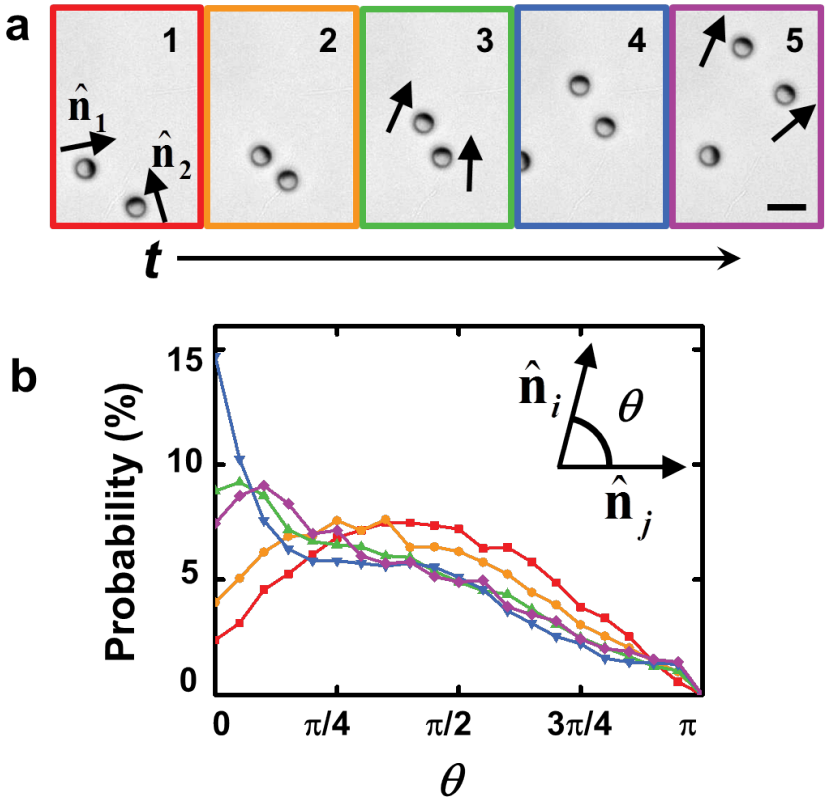

Figure S2. Quantifying binary collision events in the swarm phase. a, Snapshots of a representative collision sampled at 5 equally separated time points, showing the tendency of collision to promote transient alignment between two colliding particles. Arrows indicate the instantaneous orientation of each particle (director $\hat{\mathbf{n}}$). Time difference between two subsequent snapshots is 0.7 s. Scale bar: 5 μm. **b,** Statistics of the collision events, quantified by the time evolution of the probability distribution of θ, the angle between the orientations of the two colliding swimmers (inset). Color coding corresponds to the borders of the panels in **a**. We only count effective collisions: two particles initially head towards a common point and are separated by less than $3D$ (D the particle diameter).

4. Quantifying dipolar interaction in the cluster state

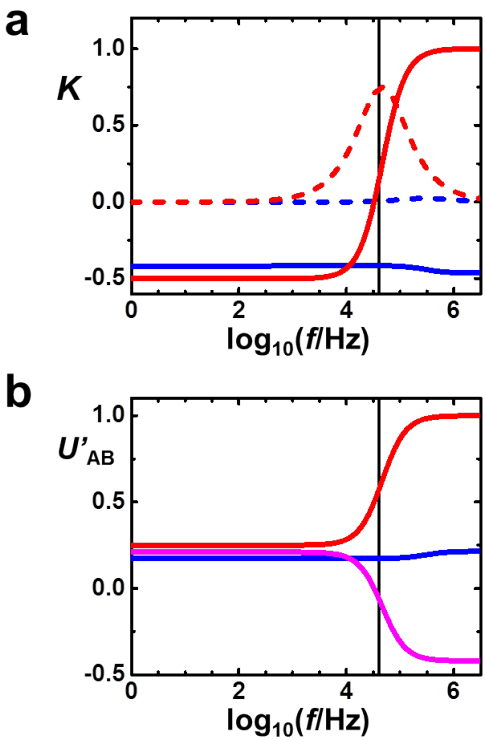

Figure S3. Dielectric spectra and interactions between Janus particles in salt solutions. **a,** Calculated complex dipole coefficient K in an 0.1 mM NaCl solution for the silica (blue) and metallic (red) hemispheres, respectively. Dashed lines correspond to the imaginary part of K and solid lines to its real part. **b,** Calculated interaction between different pairs of hemispheres. The color coding is the same as in the Fig. 2b-c of the main text. The vertical line marks the frequency $f = 40$ kHz that we used to observe the cluster state. At this frequency, the repulsion between two metallic hemispheres still dominates interparticle interactions. However, due to the presence of salt the frequency at which the particle motion reverses has shifted to 70 kHz (Supplementary Fig. S1a). Hence, in the frequency range 30-50 kHz, the particles move with their silica hemisphere forward. The resulting tail-to-tail repulsion leads to the predicted cluster state.

DOI: 10.1038/NMAT4696

5. Phenomenological model for shock-wave formation

Supplementary Fig. S4a illustrates a typical propagating polar flow. A distinct wavefront is observed, which separates the dilute, disordered region (with area fraction ϕ_{dilute}) and the dense, swarming region (with area fraction ϕ_{wave}). Based on the PIV analysis (see main text), the wavefront propagates at a speed $v_{wavefront} \approx 40$ μm/s, 1.3-1.4 times faster than the swimming Janus particles (with speed $v_{particle} = 29$ μm/s in this case) inside the polar flow. To explain this speed difference, we observe that the propagation velocity of a polar wave originates from two contributions, the directional particle motion and the recruitment of particles from the dilute phase. Within an infinitesimal time step δt, a particle within the traveling wave travels a distance $v_{particle}\delta t$. Meanwhile, the disordered phase has an average velocity of zero in the lab reference frame; hence, the Janus particles in the dilute phase move with an average speed $-v_{particle}$ relative to the wave. Physically, these particles accumulate at the wavefront and once they reach the wavefront they reorient and become part of the wave. The total number of particles joining the wave is proportional to $\phi_{dilute} \cdot v_{particle}\delta t$. As a consequence, the wavefront translates by $(1+\phi_{dilute}/\phi_{wave}) \cdot v_{particle}\delta t$, and hence $v_{wavefront} = (1+\phi_{dilute}/\phi_{wave}) \cdot v_{particle}$. Using representative numbers from Supplementary Fig. S4b, for example $\phi_{dilute} = 0.03$ and $\phi_{wave} = 0.12$ at $t = 10$ s, we estimate the ratio between the wavefront velocity and the particle velocity to be 1.25, close to the observed value.

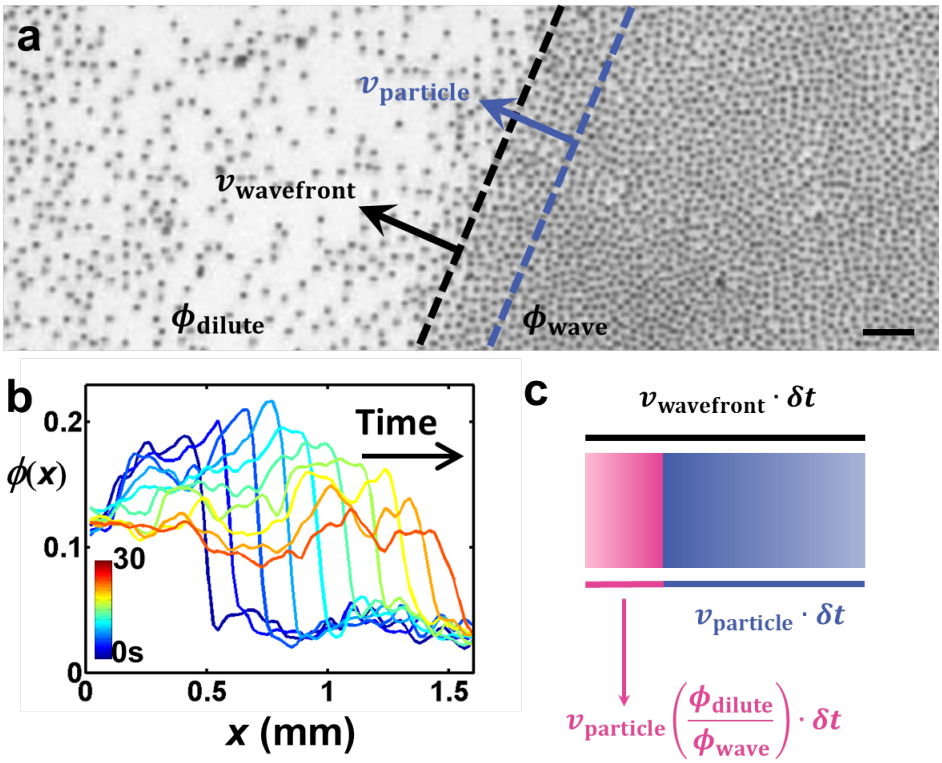

Figure S4. Propagation of the polar wave. a, Experimental snapshot of a large-scale polar wave. A sharp boundary separates the wave with a high local density ϕ_{wave} from the disordered phase with a low local density ϕ_{dilute}. The wavefront (black dashed line) propagates with velocity $v_{wavefront}$ faster than its interior Janus particles (which have velocity $v_{particle}$). Scale bar: 30 μm. **b,** Time evolution of the density profile of the polar wave. $\phi(x)$ denotes local area fraction averaged perpendicular to the propagation direction of the wave. **c,** The observed velocity of the wavefront (black) arises from two contributions: directional particle motions (blue) and recruitment of new particles from the dilute phase (pink).

DOI: 10.1038/NMAT4696

6. Collision between polar waves

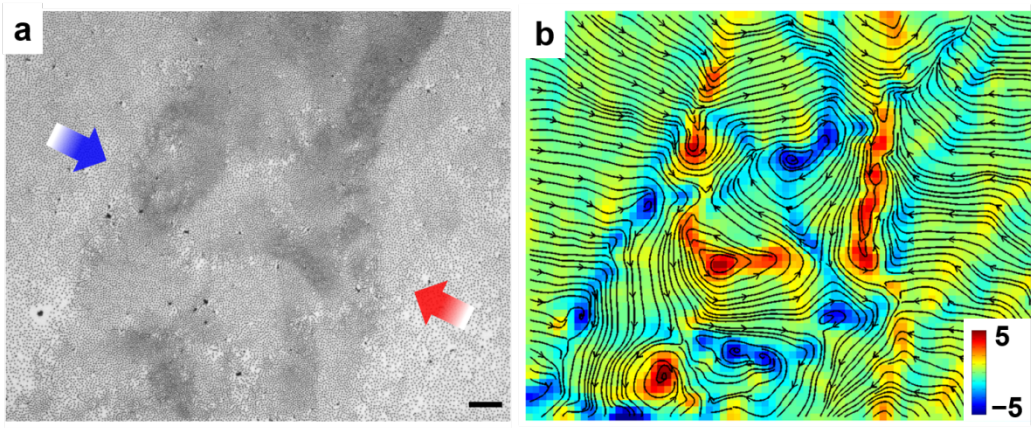

Figure S5. Collision between polar waves. a, Representative optical image of two colliding polar waves (their directions are indicated by blue and red arrows, respectively). Scale bar: 100 μm. **b,** Corresponding vorticity map $\Omega_z(\mathbf{r})$ (normalized by its spatially-averaged magnitude[24] $\langle|\Omega_z(\mathbf{r})|\rangle$). Streamlines are shown to aid visualization.

7. Time evolution in the cluster phase

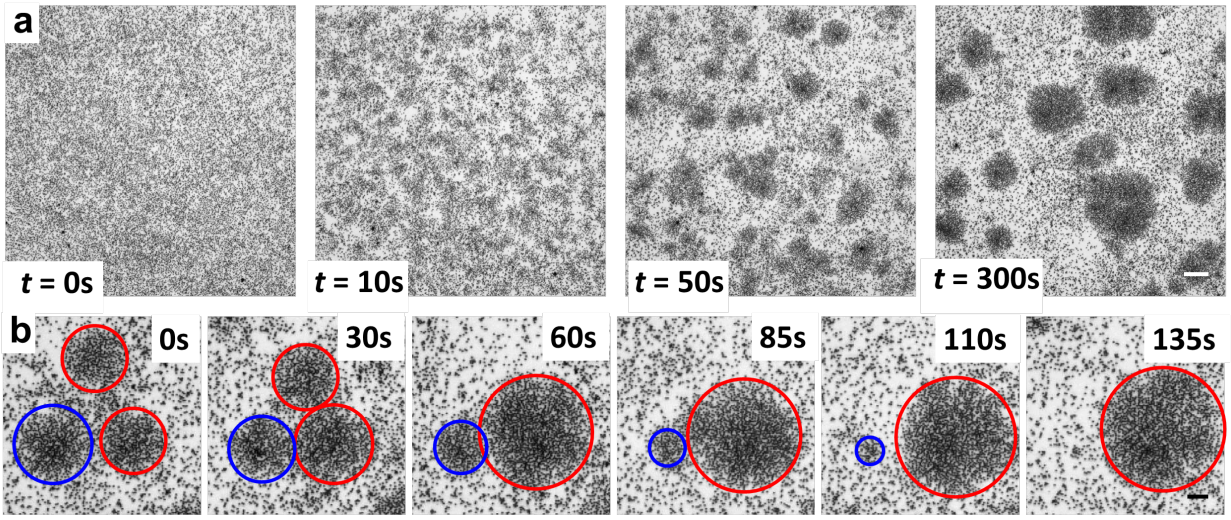

Figure S6. Time evolution in the cluster phase. a, Snapshots of cluster formation of Janus particles in an 0.1 mM NaCl solution acted upon by a 10 V, 40 kHz AC electric field. Scale bar 100 μm. **b,** Illustrative additional snapshots showing the coarsening process on a finer scale. Clusters grow primarily by merger (red circles) during the first 60 seconds, but during the following 75 seconds primarily via a process akin to Ostwald ripening in which swimming particles leave small clusters (blue circle) and join larger ones (red circle). Scale bar 40 μm.

DOI: 10.1038/NMAT4696

8. Analytical estimate of the stability limit of the chain state

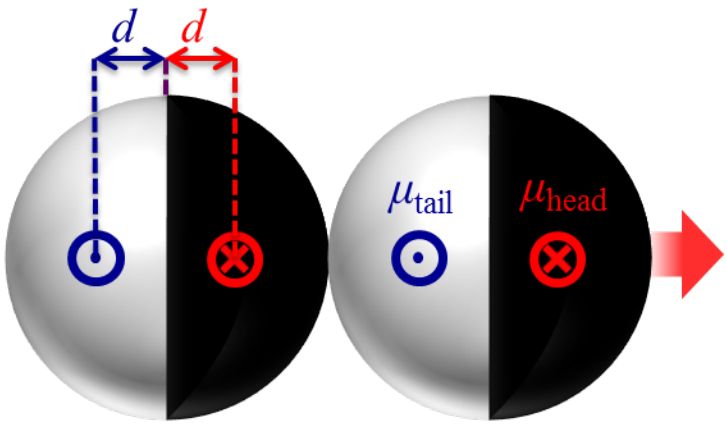

Figure S7. Representative head-to-tail configuration of two Janus particles in a chain.

In the chain state, Janus colloids concatenate by forming a head-to-tail configuration. Here we analytically estimate the phase boundaries of this state. As a first approximation, to stabilize a chain configuration, the overall dipolar force between two adjacent Janus particles (Supplementary Fig. S7), i.e., the sum of four pairwise forces between their head dipoles μ_{head} and tail dipoles μ_{tail}, should be attractive. We calculate the total force between the two particles as

$$F = -\frac{3}{4\pi\varepsilon_0}\left[\frac{\mu_{head}^2}{(2a)^4} + \frac{\mu_{tail}^2}{(2a)^4} + \frac{\mu_{head}\mu_{tail}}{(2a+2d)^4} + \frac{\mu_{head}\mu_{tail}}{(2a-2d)^4}\right],$$

where the dipole shift $d = (3/8)a$. By setting $F = 0$, we solved this quadratic equation to give $\mu_{tail}/\mu_{head} = -6.7$ or -0.15, the estimated upper and lower boundaries. The actual span observed in the simulations $(-5, -0.35)$ is close to this estimate.

9. Comparison between simulation and experiment

To compare the experimental observations with the phase diagram obtained in simulation (Fig. 4 in the main text), we need to convert the complex dipole coefficient K into a real number. We proceed by calculating the dipolar interaction. For two hemispheres A and B, the interaction is

$$U_{\mathrm{AB}} = \frac{4\pi\varepsilon_0\varepsilon_{\mathrm{s}}\,\mathrm{Re}\left(K_{\mathrm{A}}^{*}K_{\mathrm{B}}\right)a^6E_0^2}{r_{\mathrm{AB}}^3},$$

where E_0 is the amplitude of the applied field and r_{AB} the distance between their induced dipoles. We set $r_{\mathrm{AB}} = 2a$ to calculate the interaction pairs $U_{\mathrm{head\_head}}$ and $U_{\mathrm{tail\_tail}}$, and use $\sqrt{U_{\mathrm{tail-tail}}/U_{\mathrm{head-head}}}$ (taking appropriate account of the sign) as an estimate for $\mu_{\mathrm{tail}}/\mu_{\mathrm{head}}$. To obtain the experimental swimming force F_{swim}, we track the average velocity v of swimming Janus spheres, and estimate the force as $F_{\mathrm{swim}} = 6\pi\eta av$. Such calculations yield $R = \mu_{\mathrm{tail}}/\mu_{\mathrm{head}}$ equal to 0.1, 1.7 and −0.5 and $M = F_{\mathrm{rep}}/F_{\mathrm{swim}}$ equal to 15, 3, 22 for the swarming, isotropic and chaining states, respectively, in agreement with the simulation phase diagram. However, the clustering phase observed in experiment corresponds to a dipole ratio $\mu_{\mathrm{tail}}/\mu_{\mathrm{head}} = 1.9$, lower than the phase boundary predicted by the simulation. In reality, the imaginary part of the dipole coefficients gives rise to a moderate attraction between head and tail hemispheres. This aids particle aggregation by forming short, transient chains and thus reduces the requirement for the electrostatic imbalance $\mu_{\mathrm{tail}}/\mu_{\mathrm{head}}$. Nevertheless, for simplicity and generality, we use real-valued dipoles in the simulations.

DOI: 10.1038/NMAT4696

Supplementary References

31. Sharma, V., Yan, Q., Wong, C. C., Carter, W. C. & Chiang, Y.-M. Controlled and rapid ordering of oppositely charged colloidal particles. *J. Colloid Interface Sci.* **333,** 230-236 (2009).

32. Shilov, V. N., Delgado, A. V., Gonzalez-Caballero, F. & Grosse, C. Thin double layer theory of the wide-frequency range dielectric dispersion of suspensions of non-conducting spherical particles including surface conductivity of the stagnant layer. *Colloids Surf. A* **192,** 253-265 (2001).

33. Boero, M., Ikeshoji, T. & Terakura, K. Density and temperature dependence of proton diffusion in water: A first-principles molecular dynamics study. *ChemPhysChem* **6,** 1775-1779 (2005).

34. Zeebe, R. E. On the molecular diffusion coefficients of dissolved CO_2, HCO_3^-, and CO_3^{2-} and their dependence on isotopic mass. *Geochim. Cosmochim. Acta* **75,** 2483-2498 (2011).

35. Samson, E., Marchand, J. & Snyder, K. A. Calculation of ionic diffusion coefficients on the basis of migration test results. *Mat. Struct.* **36,** 156-165 (2003).

36. Garcia-Sánchez, P., Ren, Y., Arcenegui, J. J., Morgan, H. & Ramos, A. Alternating current electrokinetic properties of gold-coated microspheres. *Langmuir* **28,** 13861-13870 (2012).

37. Pascall, A. J. & Squires, T. M. Induced charge electro-osmosis over controllably contaminated electrodes. *Phys. Rev. Lett.* **104,** 088301 (2010).

38. Kijlstra, J., van Leeuwen, H. P. & Lyklema, J. Low-frequency dielectric relaxation of hematite and silica sols. *Langmuir* **9,** 1625-1633 (1993).

39. Suzuki, R., Jiang, H. R. & Sano, M. Validity of fluctuation theorem on self-propelling particles. arXiv:1104.5607 (2011).

DOI: 10.1038/NMAT4696

Titles and legends for Supplementary Movies

Supplementary Movie 1: Active chain state in 3D simulations. This movie shows growing chains of Janus particles (volume fraction 0.0077) in a 3D molecular dynamics simulation 30 seconds after swimming is initiated. A constant force is applied as described in Methods section to each particle, which carries a negative charge –200e on its leading hemisphere and a positive charge +200e on its trailing hemisphere. The movie is played 3× faster than real time and lasts 45 seconds in real units.

Supplementary Movie 2: Active swarm state in 3D simulations. This movie shows growing swarms of Janus particles (volume fraction 0.0157) in a 3D molecular dynamics simulation just after swimming is initiated. A constant force is applied as described in Methods section to each particle, which carries a strongly charged leading hemisphere (–2500e) and a neutral trailing hemisphere. The movie is played 2× faster than real time and lasts 34 seconds in real units.

Supplementary Movie 3: Active cluster state in 3D simulations. This movie shows growing clusters of Janus particles (volume fraction 0.0077) in a 3D molecular dynamics simulation just after swimming is initiated. A constant force is applied as described in Methods section to each particle, which has a neutral leading hemisphere and a highly charged trailing hemisphere (+1000e). The movie is played 3× faster than real time and lasts 24 seconds in real units.

Supplementary Movie 4: Homogeneous ("active gas") state in quasi-2D experiment. This movie shows Janus colloids (3 μm diameter), sedimented to the bottom of a sample cell in water, swimming in response to an electric field of 7 V and 5 kHz perpendicular to the image plane. The movie plays in real time. The viewing window is $95 \cdot 127\ \mu m^2$.

Supplementary Movie 5: Representative collision-induced alignment event of head-repulsive particles observed in quasi-2D experiment. This movie shows two colliding swimmers, highlighted by blue circles, swimming in response to an electric field (10 V, 30 kHz) perpendicular to the image plane. The movie plays 3× slower than real time. The viewing window is $80 \cdot 80\ \mu m^2$.

Supplementary Movie 6: Swarm state observed in quasi-2D experiment after swimming is initiated. This movie shows particles sedimented to the bottom of a sample cell in water, stimulated to swim in an electric field (10 V, 30 kHz) perpendicular to the image plane. The movie plays in real time. The viewing window is $64 \cdot 80\ \mu m^2$.

Supplementary Movie 7: Active chain state observed in quasi-2D experiment after swimming is initiated. This movie shows particles sedimented to the bottom of a sample cell in water, stimulated to swim in an electric field of 10 V and 1 MHz. Note the mixture of growing chains and rings, with the formation of a stationary rotating ring near the end of the movie. The movie plays in real time. The viewing window is $46 \cdot 60\ \mu m^2$.

Supplementary Movie 8: Active clustering observed in quasi-2D experiment after swimming is initiated. This movie shows Janus particles sedimented to the bottom of a sample cell in an 0.1 mM NaCl solution and stimulated to swim in an electric field (10 V, 40 kHz) perpendicular to the image plane. The movie plays 20× faster than real time. The viewing window is $380 \times 506\ \mu m^2$.

Supplementary Movie 9: Polar wave observed in quasi-2D experiment. This movie shows the formation of propagating wave of collectively swarming Janus colloids observed with a 5· objective within a large view window of $1215 \cdot 1620\ \mu m^2$ while swimming in an electric field (10 V, 30 kHz) perpendicular to the image plane. The first half of the movie, played at 4× real

DOI: 10.1038/NMAT4696

time, demonstrates the evolution from small swarms into a large polar wave. The second half, played at 4× real time, shows a shock wave sweeping over the field of view at a later stage.

Supplementary Movie 10: Vortex observed in quasi-2D experiment. This movie shows a giant vortex formed in the late stage of the swarm state, for particles sedimented to the bottom of a sample cell and swimming in an electric field (10 V, 30 kHz) perpendicular to the image plane. The movie plays 6× faster than real time. The viewing window is $1215 \cdot 1620\ \mu m^2$.